ISSN 1070-3284, Russian Journal of Coordination Chemistry, 2022, Vol. 48, No. 1, pp. 16–25. © Pleiades Publishing, Ltd., 2022.
Russian Text © The Author(s), 2022, published in Koordinatsionnaya Khimiya, 2022, Vol. 48, No. 1, pp. 18–28.

Electron Density Distribution in the Crystal of the Biocompatible Metal–Organic Framework

A. A. Ishchenko[a, b], A. M. Pak[a], and Yu. V. Nelyubina[a, b, *]

[a] *Nesmeyanov Institute of Organoelement Compounds, Russian Academy of Sciences, Moscow, 119991 Russia*
[b] *Moscow Institute of Physics and Technology (National Research University), Dolgoprudnyi, Moscow oblast, Russia*
**e-mail: unelya@ineos.ac.ru*

Received May 11, 2021; revised June 2, 2021; accepted June 3, 2021

Abstract—The earlier described organic coordination polymer $[Zn_3(HCit)_2(H_2O)_2]_n$ (HCit is citric acid) (**I**) formed completely by the biocompatible components is synthesized under hydrothermal conditions. The selection of the hydrothermal synthesis conditions makes it possible to obtain the polymer as high-quality single crystals and perform a detailed analysis of the electron density distribution function recovered using the data of a high-resolution X-ray diffraction experiment. This study is the second example of such investigations for the biocompatible metal–organic framework.

Keywords: metal–organic framework, electron density distribution, X-ray diffraction, solvothermal synthesis, topological analysis, functional packing

DOI: 10.1134/S107032842201002X

INTRODUCTION

Metal–organic frameworks (MOF) [1] represent a unique class of crystalline materials, whose periodical structures are formed by metal ions or clusters, which act as metal-containing units, and coordinated ligands acting as organic linkers. A similar combination of organic and inorganic moieties can be chosen in rather broad ranges, which makes it possible to prepare similar materials with specified physicochemical properties (e.g., porosity [2]). This provides their use in gas storage [3] and separation [4], as proton-conducting membranes [5] and catalysts or their "containers" in various chemical processes [6], and even in structural biology [7]. In addition, MOF formed by biocompatible components are actively applied in medicine [8], primarily for the controlled release of therapeutic agents, including those incorporated in MOF as organic linkers [9], and for the production of optical sensors and contrast agents for magnetic resonance tomography [10]. The possibility of using crystalline materials of this type for the preparation of functional food wrapping has recently been shown [11, 12].

The solvothermal synthesis is one of the popular methods for the synthesis of MOF [13] and makes it possible to obtain high-quality single crystals suitable to determine the crystal structure [14] (and even the electron density distribution in them [15–18]) using X-ray diffraction (XRD). In this work, we used this method to synthesize the earlier described [19–22] MOF $[Zn_3(HCit)_2(H_2O)_2]_n$ (HCit is citric acid) (**I**) (Scheme 1) containing only biocompatible components: coordinated water molecules, reaction products of zinc acetate playing the key role in many physiological processes [23, 24], and citric acid widely used in food industry [25]. The synthesized crystalline product was isolated in the individual form and characterized by elemental analysis and XRD. In addition, a high-resolution XRD experiment was carried out for high-quality single crystals of compound **I** formed under the chosen hydrothermal conditions, and the XRD data were used for the examination of the experimental electron density distribution in the crystal of the synthesized MOF.

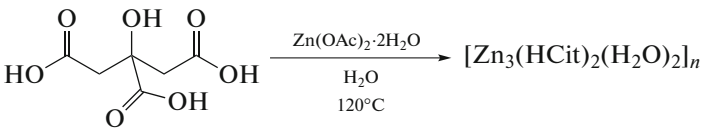

H_4Cit

Scheme 1.

Similar studies are rather rare for this class of crystalline materials [26–28] primarily because of the harsh requirements imposed on the quality of the studied sample. Among these requirements are the following: a single crystal of a large size rarely achieved even for simple organic compounds and the absence of disordered fragments, which is especially problematic for porous MOF containing solvent or other guest molecules (often disordered) in the pores [15, 17, 29]. As a result, there are a few examples of studies of the electron density distribution recovered from the high-resolution XRD data in crystals of MOF, and almost all of them [17, 30–32] used a more intensive synchrotron radiation [15, 16, 18, 33–35]. Among them $[Zn(HCOO)_2(H_2O)_2]$ [30] is the only MOF formed by the biocompatible components that include water molecules and formic acid anions along with the zinc(II) ion. Formic acid is used as a preserving agent and biologically active additive in food industry [36, 37].

In this work, the experimental electron density distribution was examined for a single crystal of $[Zn_3(HCit)_2(H_2O)_2]_n$ (**I**) obtained under the hydrothermal conditions, which is the second example of a similar study for the biocompatible MOF.

EXPERIMENTAL

All procedures related to the synthesis of the complex were carried out in air using commercially available organic solvents and reagents. Analyses for the carbon and hydrogen contents were conducted on a CarloErba microanalyzer (model 1106). Compound **I** was synthesized using a modified procedure [19] under the hydrothermal conditions (Scheme 1).

Synthesis of $[Zn_3(HCit)_2(H_2O)_2]_n$ (I). A mixture of citric acid (0.1921 g, 1 mmol) and $Zn(OAc)_2{\cdot}2H_2O$ (0.2195 g, 1 mmol) was dissolved in distilled water (1 mL), and the solution was heated in a sealed glass ampule to 120°C with a rate of 200°C/h and held at this temperature for 24 h followed by slow cooling to room temperature for 5 h. The obtained colorless prismatic crystals, one of which was taken for XRD and returned after the XRD experiment, were separated from the mother liquor, washed with distilled water and ethanol, and dried in air. The yield of compound **I** was 0.153 g (75%).

For $C_{12}H_{14}O_{16}Zn_3$		
Anal. calcd., %	C, 23.61	H, 2.31
Found, %	C, 23.58	H, 2.19

XRD. The XRD study of a single crystal of compound **I** taken from the sealed glass ampule immediately after cooling to room temperature was carried out at 120 K on a Bruker APEX2 DUO CCD diffractometer (MoK_α radiation, graphite monochromator, ω scan mode). The structure was solved using the ShelXT program [15] and refined by full-matrix least squares against F^2_{hkl} using the Olex2 program [16] in the anisotropic approximation for non-hydrogen atoms. Hydrogen atoms were localized from the difference Fourier electron density syntheses and refined in the isotropic approximation. Selected crystallographic data and structure refinement parameters are given in Table 1.

The full set of XRD parameters for compound **I** was deposited with the Cambridge Crystallographic Data Centre (CIF file CCDC no. 2082522; http://www.ccdc.cam.ac.uk/).

The multipole refinement of **I** was performed in terms of the Hansen–Coppens formalism [38] using the XD software [39] with the cage and valence electron densities obtained from the wave functions based on the relativistic solution of the Dirac–Fock equation. Prior to the refinement, the C–H bond lengths were normalized to standard neutronographic values [40] of 1.091 Å, O–H of the hydroxyl group were normalized to 0.970 Å [40], and O–H were normalized to a value of 0.972 Å obtained from the neutronographic data for similar structures [41]. The anisotropic thermal parameters of hydrogen atoms were estimated using the Shade3 Server program [42]. The multipole expansion for zinc, carbon, and oxygen atoms was restricted by the hexadecapole level, and that for hydrogen atoms was restricted by the dipole level. The refinement was performed against F_{hkl}. All covalently bound pairs of atoms satisfied the Hirschfeld criterion [43] for bond hardness. The corresponding values did not exceed 9×10^{-4} Å^2. The multipole refinement results are as follows: $R = 0.0172$, $Rw = 0.0140$, and GOOF = 1.0048 for 11633 reflections with $I > 3\sigma(I)$. The residual electron density did not exceed 0.29 e Å^{-3}. The character of the dependence of the fractal dimensionality d^f on ρ_0 obtained from the residual density analysis results [44] (Fig. 1) demonstrates slight deviations from the Gaussian distribution of the residual electron density indicating that the parameters of the multipole Hansen–Coppens model obtained by the refinement are "adequate" [45].

The approximation of the Thomas–Fermi theory [46] was used for the calculation of $v(\mathbf{r})$ from the XRD data. According to this approach, the kinetic energy density $g(\mathbf{r})$ can be obtained from the equation $g(\mathbf{r}) = 3/10(3\pi^2)^{2/3}[\rho(\mathbf{r})]^{5/3} + (1/72)|\nabla\rho(\mathbf{r})|^2/\rho(\mathbf{r}) + 1/6\nabla^2\rho(\mathbf{r})$, which in combination with the local virial theorem [47] $2g(\mathbf{r}) + v(\mathbf{r}) = 1/4\nabla^2\rho(\mathbf{r})$ makes it possible to calculate both the potential energy density $v(\mathbf{r})$ and local energy density $h_e(\mathbf{r})$. The search for critical points (CP) (3, –1) and the calculation of the topological characteristics $\rho(\mathbf{r})$ (including $h_e(\mathbf{r})$, $g(\mathbf{r})$, and $v(\mathbf{r})$) were performed using the WinXPRO program [48].

Table 1. Selected crystallographic data and structure refinement parameters of compound **I**

Parameter	Value
Empirical formula	$C_{12}H_{14}O_{16}Zn_3$
FW	610.34
Crystal system	Monoclinic
Space group	$P2_1/c$
Z	2
a, Å	6.11710(10)
b, Å	14.5347(3)
c, Å	9.5647(2)
β, deg	102.4480(10)
V, Å^3	830.41(3)
ρ_{calc}, g cm^{-3}	2.441
μ, cm^{-1}	43.95
F(000)	608
$2\theta_{max}$, deg	120
Number of measured reflections	262359
Number of independent reflections	12523
Number of reflections with $I > 2\sigma(I)$	11184
Number of refined parameters	170
R_1 (for reflections with $I > 2\sigma(I)$)	0.0214
wR_2 (for all reflections)	0.0501
GOOF	1.073
Residual electron density ($\Delta\rho_{min}/\Delta\rho_{max}$), e Å^{-3}	−0.759/1.392

RESULTS AND DISCUSSION

The MOF $[Zn_3(HCit)_2(H_2O)_2]_n$ (**I**) has previously been synthesized under the solvothermal conditions by holding the zinc salt with citric acid in an aqueous medium or in various ethanol–water mixtures in the temperature range from 140 to 200°C. The synthesis time was varied from 16 to 72 h, and the ratio of the zinc salt (zinc(II) acetate, nitrate, or sulfate) to citric acid was chosen in the range from 1 : 1 to 1 : 1.5 [19–22]. Although the solvent chosen and the ratio of the starting reactants did not affect the formation of compound **I**, it was not necessary to control the pH of the solution by the addition of a base, for example, alkali or ammonia, when zinc(II) acetate was used. For this reason, compound **I** was synthesized from zinc(II) acetate and citric acid under the hydrothermal conditions (Scheme 1) using a modified procedure [19]. The use of a lower temperature (120 instead of 200°C [19]) and a shorter synthesis time (24 instead of 72 h [19]) made it possible to synthesize the target product in a higher yield (75 instead of 63% [19]) and to obtain high-quality single crystals of this MOF for the high-resolution XRD study.

As mentioned previously [19–22], compound **I** is a 2D coordination polymer (Fig. 2) in which the role of the metal-containing units is played by two symmetry-independent zinc(II) ions and water molecules. The zinc(II) ions exist in different environments of the citric acid anions, are deprotonated over three carboxyl groups, and perform the function of organic linkers.

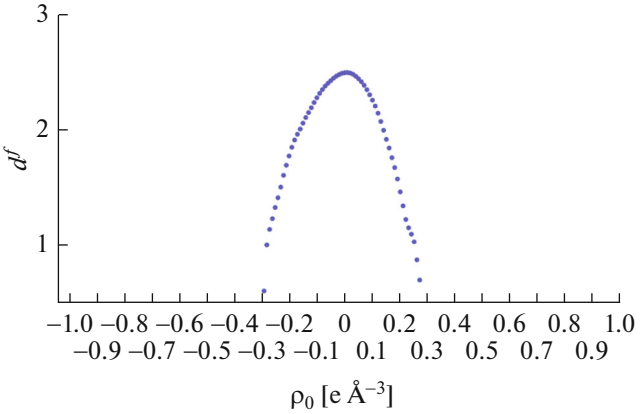

Fig. 1. Fractal dimensionality d^f vs. residual electron density ρ_0 for the electron density distribution in compound **I** obtained by the multipole refinement of the high-resolution XRD data.

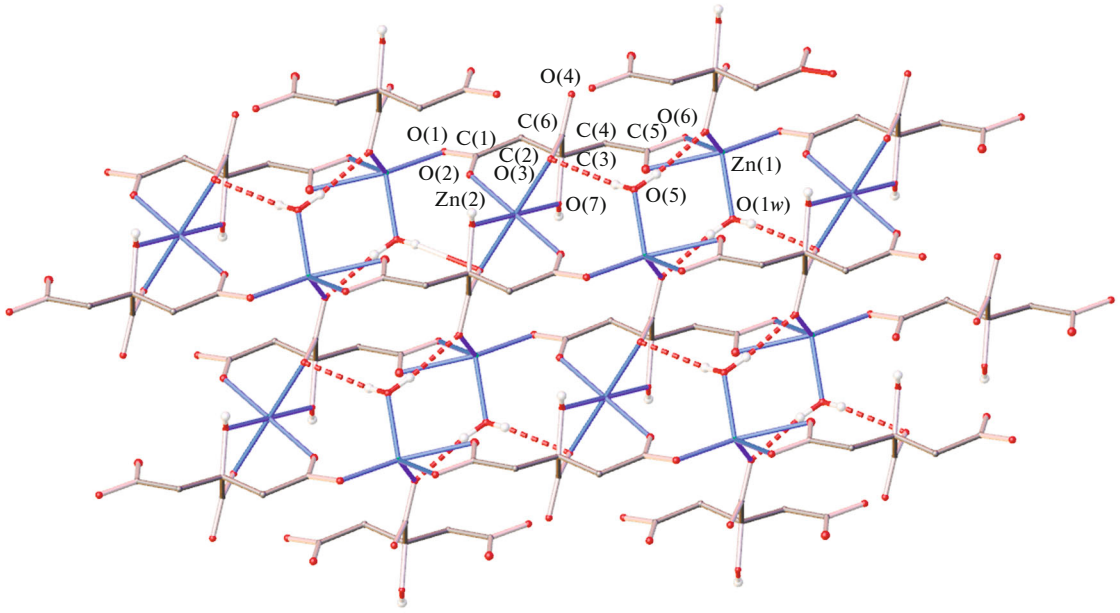

Fig. 2. Fragment of the crystal packing in compound **I** illustrating the packing of the 2D coordination layer. The hydrogen atoms of the CH_2 groups are omitted for clarity, and only symmetry-independent atoms are enumerated.

The shape of the coordination polyhedron of the Zn(1) ion is close to a distorted trigonal bipyramid (Table 2) in which the equatorial positions are occupied by the O(4) and O(6) oxygen atoms of two carboxyl groups (Zn–O 2.0170(4) and 2.0623(4) Å) and one water molecule (Zn–O 2.0342(4) Å) and the axial positions are occupied by the O(1) and O(5) oxygen atoms of the carboxyl groups (Zn–O 1.9749(4) and 2.3197(4) Å) of the citric acid anion. On the contrary, the Zn(2) ion that occupies the partial position (inversion center) in the crystal is characterized by the (pseudo)octahedral environment formed by the oxygen atoms of four carboxyl (Zn–O 2.0422(4) and 2.0829(3) Å) and two hydroxyl (Zn–O 2.1207(3) Å) groups of the anion. For the quantitative description of the shape of the corresponding polyhedra, we also used the "symmetry measures" [49] that characterize a deviation from an ideal trigonal bipyramid S(TBPY-5) and an ideal octahedron S(OC-6) (Table 2). The lower these values, the better the description of the polyhedron shape by a chosen polyhedron. In the synthesized MOF **I**, the values of S(TBPY-5) and S(OC-6) estimated from the XRD data using the Shape 2.1 program [49] are 3.893 and 0.966 for the Zn(1) and Zn(2) ions, respectively. For comparison, the deviation of the shapes of the coordination polyhedra from alternative polyhedra with five and six vertices (square pyramid (SPY-5) and trigonal prism (TP-6)) are appreciably higher (5.026 and 15.602) indicating that they can correctly be described by a distorted trigonal bipyramid and a nearly ideal octahedron.

The listed above coordination bonds with the citric acid anion acting as the organic linker result in the formation of a 2D coordination layer along the crystallographic plane *ac* (Fig. 2) additionally stabilized by the hydrogen bonds between the water molecule coordinated to the Zn(1) ion and carboxyl groups of this anion (O...O 2.8450(5) and 3.0317(5) Å, OHO 173.6(18)° and 157.0(17)°). The strong hydrogen bond between the hydroxyl group and one of the carboxyl groups (O...O 2.6454(4) Å, OHO 170.0(16)°) joins the 2D coordination layers between each other into a dense 3D carcass (Fig. 3) with the maximum pore volume lower than 2.15 $Å^3$ as follows from the XRD data estimation in the OLEX2 program [50].

A high resolution of the indicated (precision) data, which was achieved for the single crystal of **I** formed under the chosen hydrothermal synthesis conditions, allowed us to obtain both the atomic coordinates and related structural parameters discussed earlier [19–22] and the full distribution of the electron density (ED) determining all properties of crystalline materials [45], for example, magnetic properties that often serve as the object of similar studies for MOF [15, 30, 31, 33]. In spite of the problems that appear [15, 17, 29] and substantially restrict the number of similar studies, the experimental ED distribution for compound **I** obtained by the multipole refinement of the XRD data (see Experimental) is characterized by all expected properties. In particular, the maxima of the deformation ED (DED) are observed at the middles of the covalent bonds in the citric acid anion and at the oxygen atoms of the hydroxyl group and carboxyl groups of this anion and the water molecule in the positions

Table 2. Selected geometric parameters of compound **I**

Parameter*	Zn(1)	Zn(2)
$M-O_{COO}$, Å	1.9749(4)–2.3197(4)	2.0422(4), 2.0829(3)
$M-O_{OH}$, Å		2.1207(3)
$M-O_{H_2O}$, Å	2.0342(4)	
S(TBPY-5)	3.893	
S(SPY-5)	5.026	
S(OC-6)		0.966
S(TP-6)		15.602

* O_{COO}, O_{OH}, and O_{H_2O} are the oxygen atoms of the carboxyl and hydroxyl groups of the citrate anion and water molecules, and S(TBPY-5), S(SPY-5), S(OC-6), and S(TP-6) are the deviations of the polyhedron shape of the metal atom from a trigonal bipyramid (TBPY-5), a square pyramid (SPY-5), an octahedron (OC-6), and a trigonal prism (TP-6).

corresponding to two lone electron pairs (Fig. 4). The latter (except for those belonging to the O(2) and O(3) atoms [51]) are directed toward the areas of DED accumulation at the zinc ions, which has previously been observed for the second biocompatible MOF $[Zn(HCOO)_2(H_2O)_2]$ [30] studied using the same approach. However, in our case, the DED distribution around two symmetry-independent zinc ions existing in the trigonal bipyramidal and (pseudo)octahedral (as in $[Zn(HCOO)_2(H_2O)_2]$ [30]) environments is distinguished by a more pronounced asymmetry (Fig. 5) resembling 3*d* orbitals of transition metals like in some other zinc(II) complexes [51–53]. The population of the corresponding orbitals (Table 3) of two zinc ions in MOF **I** estimated from the multipole refinement results of the high-resolution XRD data is consistent with their completely occupied 3*d* shell (9.99(2) and 9.98(2) e) indicating an important role of 4*s* electrons

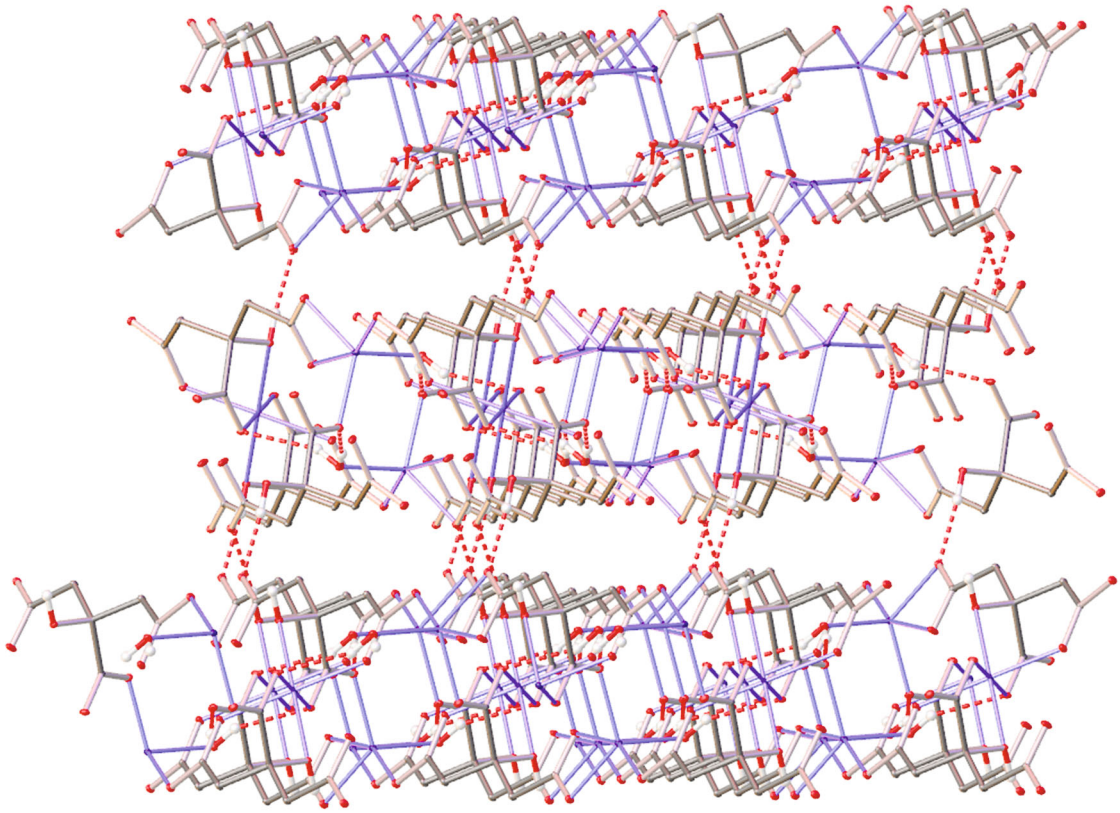

Fig. 3. Fragment of the crystal packing in compound **I** illustrating the packing of the 2D coordination layers in the crystal. The hydrogen atoms of the CH_2 groups are omitted for clarity.

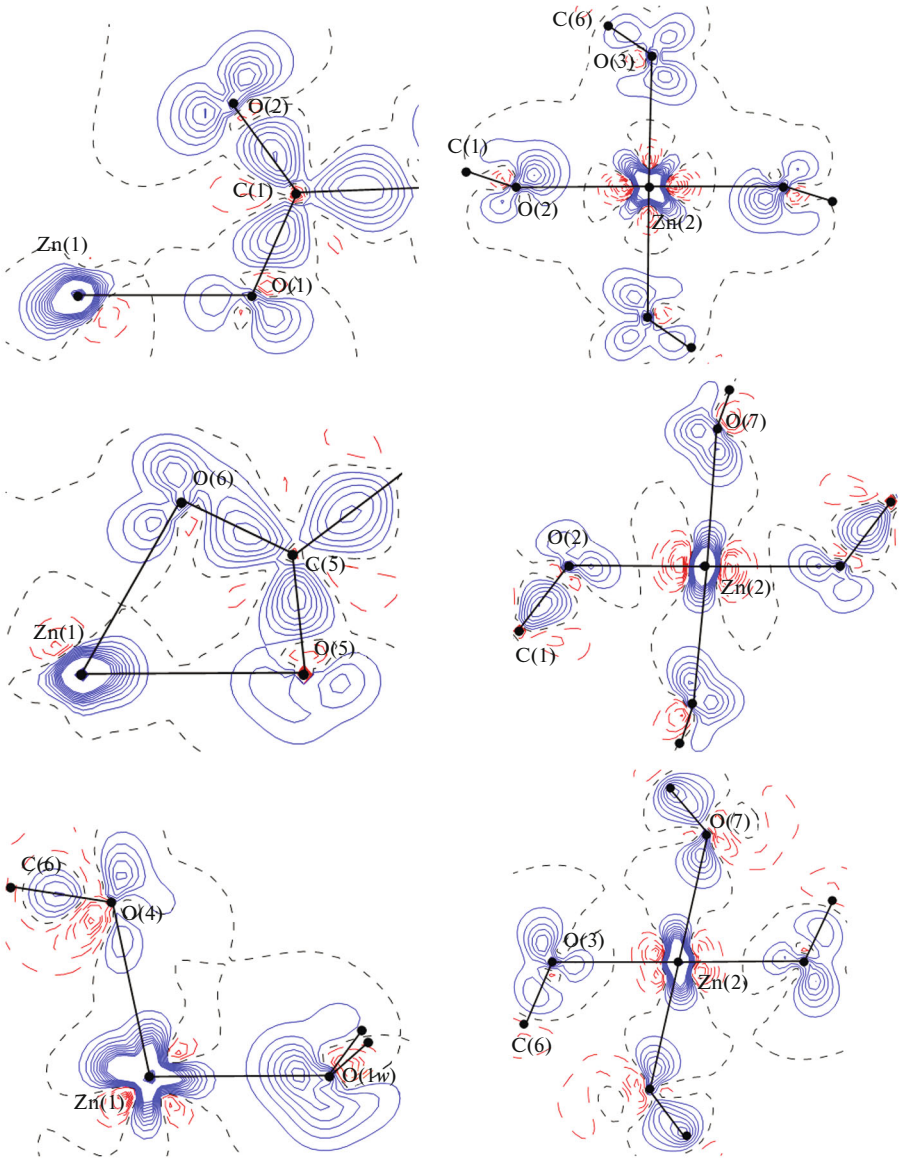

Fig. 4. Two-dimensional DED distributions in the area of the coordination bonds formed by the (left) Zn(1) and (right) Zn(2) atoms in the crystal of compound **I**. The contours are performed with an increment of 0.1 e Å^3, and the corresponding positive and negative values are shown by blue and red, respectively.

in the metal–ligand binding. This is indirectly indicated by their charges (+0.87 and +0.94 e) obtained by an analysis of the ED distribution in terms of the "Atoms in Molecule" theory [47] (Table 4). The charges are close to those in the MOF $[Zn(HCOO)_2(H_2O)_2]$ (+0.90 and +0.94 e [30]). The coordinated water molecule is also nearly neutral [30], whereas the charge of the citric acid anion with three deprotonated carboxyl groups is –1.30 e.

Another feature of MOF **I** that was earlier met for the MOF [30] and zinc(II) complexes [51] is inequal populations of five formally occupied 3*d* orbitals of both symmetry-independent zinc ions (Table 3). For example, the Zn(1) ion in the distorted trigonal bipyramidal environment is characterized by the preferable population of the d_{x2-y2}, d_{xz}, and d_{z2} orbitals oriented toward the ligands, which is consistent with the direction of the lone electron pairs of the latter toward the ED accumulations at the metal ion (Fig. 4). On the contrary, the d_{x2-y2} and d_{z2} orbitals of the Zn(2) ion turned out to be the least and most populated, which agrees with the corresponding ED accumulations oriented toward the lone electron pairs of the axial O(7) oxygen atoms but not toward similar pairs of the equatorial oxygen atoms O(2) and O(3) (Fig. 4). Thus, a mixed scenario of the ED distribution in the area of coordination bonds takes place in the crystal of MOF **I** simultaneously combining two opposite variants ear-

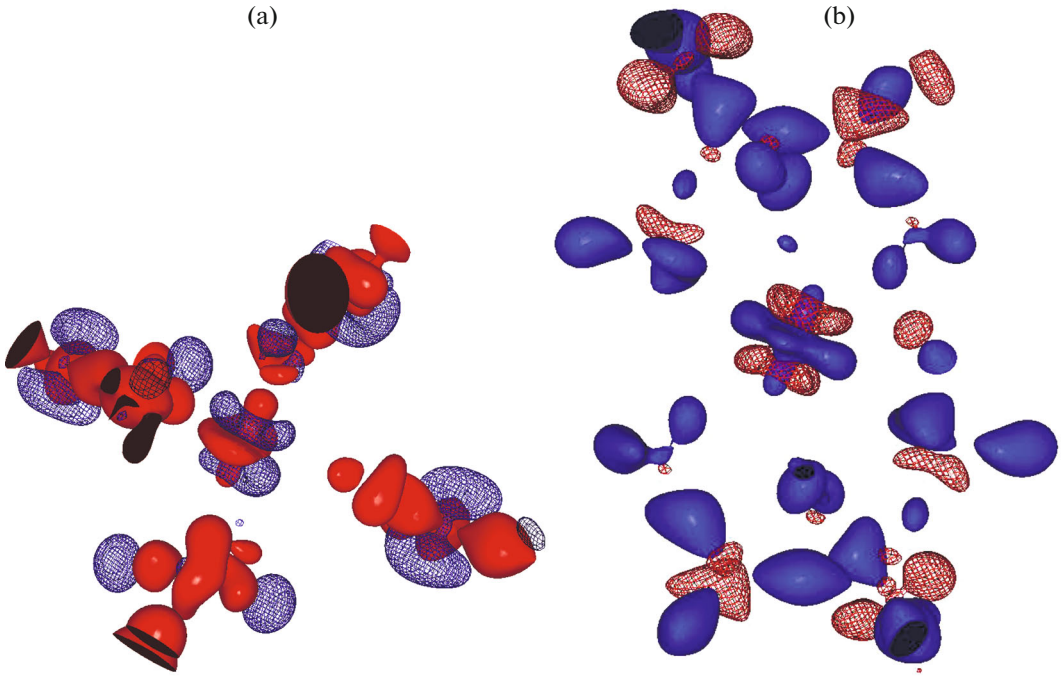

Fig. 5. Isosurface of the 3D DED distribution (values of 0.3 and –0.3 e Å^{-3} are shown by blue and red, respectively) around the (a) Zn(1) and (b) Zn(2) atoms in the crystal of compound **I**.

lier found for the (pseudo)octahedral zinc(II) complexes [51–53].

The observed difference in the populations of the 3*d* orbitals, charges, and volumes (12.2 and 10.7 Å^3) of two symmetry-independent zinc ions (Tables 3, 4) shows different coordination environments of these two ions, one of which, Zn(1), forms the shortest and longest coordination bonds.

The topological analysis of the ED distribution in the crystal of MOF **I** in terms of the "Atoms in Molecule" theory [47] revealed the CP (3, –1) ascribed to the binding interactions [55, 56] for the above described coordination and hydrogen bonds inside the 2D coordination layers and between them and also for a series of weaker contacts (Table 5). In all cases, the Zn–O coordination bonds are classified as interactions that occupy an intermediate position between the generalized interactions characteristic of covalent bonds (e.g., in the citric acid anion) and interactions of closed shells typically exemplified by weak van der Waals contacts. This is indicated by positive Laplacian $\nabla^2\rho(\mathbf{r})$ (3.63–9.52 e Å^{-5}) and negative electron energy density $h_e(\mathbf{r})$ (from –0.0112 to –0.0012 a.u.) at the CP (3, –1) of the coordination bonds similar to those in the MOF $[Zn(HCOO)_2(H_2O)_2]$ [30]. The shortest Zn(1)–O(1) bond ($\rho(\mathbf{r})$ = 0.55 e Å^{-3}, $\nabla^2\rho(\mathbf{r})$ = 9.52 e Å^{-5}, $h_e(\mathbf{r})$ = –0.0112 a.u.) is expectedly the strongest of them, and its energy estimated from the successfully used for this purpose correlation [57] with the potential energy density at the CP (3, –1) [58, 59] reaches 38.0 kcal/mol. For comparison, the energy of the weakest coordination bond ($\rho(\mathbf{r})$ = 0.27 e Å^{-3}, $\nabla^2\rho(\mathbf{r})$ = 3.63 e Å^{-5}, $h_e(\mathbf{r})$ = –0.0012 a.u.) with the O(5) atom occupying the axial position maximally remote from the Zn(1) ion in the trigonal bipyramidal environment is 12.6 kcal/mol. The observed linear relationship (with the approximation reliability $R^2 = 0.90$) between the energy and metal–ligand distance along with low negative values of $h_e(\mathbf{r})$ at the

Table 3. Populations of the 3*d* orbitals of the zinc(II) ions in the crystal of compound **I***

Cation	d_{z2}	d_{xz}	d_{yz}	d_{x2-y2}	d_{xy}	Σ
Cation Zn(1)	2.04(1)	2.07(1)	1.81(1)	2.17(1)	1.90(1)	9.99(2)
Cation Zn(2)	2.14(1)	2.02(1)	1.97(1)	1.73(1)	2.12(1)	9.98(2)

* The populations of the 3*d* orbitals were calculated in terms of the standard approach [54] using the XD2016 program [39] for the choice of the local axes *z* and *y* for the Zn(1) and Zn(2) ions in the trigonal bipyramidal and octahedral environments along the Zn(1)–O(1), Zn(1)–O(1*w*), Zn(2)–O(7), and Zn(2)–O(2) bonds with the oxygen atoms that occupy the axial and equatorial positions in the trigonal bipyramid and octahedron, respectively, and along the *x* axis perpendicularly to the indicated directions.

Table 4. Total charges and volumes of the ions and water molecules in the crystal of compound **I***

Ion/molecule	Charge, e	Volume, Å^3
Cation Zn(1)	+0.87	12.2
Cation Zn(2)	+0.94	10.7
Anion	−1.30	168.4
Water	−0.02	21.0

* "Charge loss" due to the numerical integration of the ρ(**r**) function by atomic basins did not exceed 0.02 e, and the formula unit volume reproduced the volume of the independent part of the unit cell (the corresponding difference did not exceed 0.4%).

CP (3, −1) indicates the predominantly ionic nature of these interactions but with some contribution of the covalent component as in the MOF $[Zn(HCOO)_2(H_2O)_2]$ [30]. Interestingly, the energy of all coordination bonds formed by two symmetry-independent zinc ions in different coordination environments takes rather close values of 147.3 and 152.5 kcal/mol.

Other interactions responsible for the formation of 2D coordination layers in addition to covalent and coordination bonds and for their binding with each other in the crystal of compound **I** are classified as interactions of closed shells characterized by positive Laplacian $\nabla^2\rho(\mathbf{r})$ and electron energy density $h_e(\mathbf{r})$ at the corresponding CP (3, −1). The strongest interaction (with an energy of 13.9 kcal/mol) exceeding in strength the above described long coordination bond Zn(1)–O(5) is the hydrogen bond between the hydroxyl and carboxyl groups ($\rho(\mathbf{r})$ = 0.26 e Å^{-3}, $\nabla^2\rho(\mathbf{r})$ = 5.53 e Å^{-5}, $h_e(\mathbf{r})$ = 0.0065 a.u.) of the citric acid anions from the adjacent coordination layers. The hydrogen bonds formed by the water molecule inside the layer reach appreciably lower energies of 4.3 and 1.8 kcal/mol ($\rho(\mathbf{r})$ = 0.06 and 0.04 e Å^{-3}, $\nabla^2\rho(\mathbf{r})$ = 3.37 and 1.29 e Å^{-3}, $h_e(\mathbf{r})$ = 0.0107 and 0.0039 a.u.). Similar differences are well described by an exponential dependence of the energy on the distance between the hydrogen atom and its acceptor (with the approximation reliability $R^2 = 0.98$) similarly to that observed earlier for hydrogen bonds [60]. One of two hydrogen

Table 5. Topological parameters of the ρ(**r**) function at the CP (3, −1) corresponding to different types of interatomic interactions in the crystal of compound **I**

Interaction	*d*, Å*	ρ(**r**), e Å^{-3}	$\nabla^2\rho(\mathbf{r})$, e Å^{-5}	$h_e(\mathbf{r})$, a.u.	−v(**r**), a.u.	E_{int}, kcal/mol
Coordination bonds						
Zn(1)–O(1)	1.974	0.55	9.52	−0.0112	0.1211	38.0
Zn(1)–O(1*w*)	2.036	0.52	8.67	−0.0100	0.1100	34.5
Zn(1)–O(4)	2.017	0.52	8.75	−0.0093	0.1100	34.3
Zn(1)–O(5)	2.321	0.27	3.63	−0.0012	0.0400	12.6
Zn(1)–O(6)	2.062	0.45	7.45	−0.0057	0.0888	27.9
Zn(2)–O(2)	2.084	0.41	6.54	−0.0046	0.0771	24.2
Zn(2)–O(3)	2.042	0.44	7.79	−0.0038	0.0884	27.8
Zn(2)–O(7)	2.121	0.41	6.54	−0.0048	0.0774	24.3
Hydrogen bonds inside layer						
O(3)...H(1*wA*)	2.120	0.04	1.29	0.0039	0.0056	1.8
O(4)...H(1*wB*)	1.877	0.06	3.37	0.0107	0.0137	4.3
Hydrogen bonds between layers						
O(6)...H(7)	1.687	0.26	5.53	0.0065	0.0445	13.9
Weak interactions inside layer						
O(1*w*)...H(2*B*)	2.308	0.04	1.20	0.0035	0.0054	1.7
O(1*w*)...C(5)	3.505	0.03	0.34	0.0008	0.0019	0.6
O(2)...O(2)	3.354	0.03	0.40	0.0011	0.0020	0.6
O(7)...H(2*A*)	2.834	0.03	0.42	0.0012	0.0020	0.6
Weak interactions between layers						
O(1)...H(4*A*)	2.578	0.03	0.70	0.0020	0.0033	1.0
O(1)...C(5)	3.461	0.02	0.32	0.0009	0.0016	0.5
O(6)...H(2*A*)	2.900	0.03	0.41	0.0011	0.0021	0.6

* In all cases, the distance between the directly bound atoms is indicated.

bonds in the 2D coordination layer is comparable in energy with additional weak contacts involving oxygen atoms, for example, C–H...O (Table 5), whose energy ranges from 0.5 to 1.7 kcal/mol. The total energy of the interactions (joining the 2D coordination layers with each other) per formula unit $[Zn_3(HCit)_2(H_2O)_2]$ takes a fairly noticeable value of ~32 kcal/mol. Correspondingly, they can make an important contribution to the high thermal stability of this MOF [22] retaining its integrity on heating up to 283°C unlike its 1D and 2D analogs with other metals containing citrate anions and coordinated water molecules but having different crystal structures.

Thus, using the hydrothermal synthesis conditions we succeeded to synthesize the MOF $[Zn_3(HCit)_2(H_2O)_2]_n$ in a higher yield and also as single crystals suitable for both routine XRD (which is a certain advantage of the solvothermal method [14]) and high-resolution investigation of the experimental ED distribution [15–18]. The present study revealing, for example, the mixed type of the ED distribution [51–53] in the area of the Zn–O coordination bonds (Fig. 4) is the second example of the MOF completely formed by the biocompatible components (in addition to $[Zn(HCOO)_2(H_2O)_2]$ [30]). There are problems that substantially restrict the number of similar works for this unique [1] class of crystalline materials (first of all, those caused by disordered solvent molecules in the pores [15, 17, 29]) by the selection of the synthesis and activation conditions [17] and also using high-performance approaches [61]. The problem can be solved by the search for alternative variants of the "reconstruction" of the ED distribution associated with the use of the transferable atom model or its analogs [17, 62]. This makes it possible to understand various practically important properties (e.g., magnetic properties [15, 30, 31, 33]) of MOF and methods for controlling them by the "crystal engineering" methods [63, 64] in more detail.

ACKNOWLEDGMENTS

The elemental analysis of the synthesized product was performed under the support of the Ministry of Science and Higher Education of the Russian Federation using the equipment of the Center for Molecular Composition Studies at the Nesmeyanov Institute of Organoelement Compounds (Russian Academy of Sciences).

FUNDING

This work was supported by the Russian Science Foundation, project no. 20-73-10200.

CONFLICT OF INTEREST

The authors declare that they have no conflicts of interest.

REFERENCES

1. Yaghi, O. and Li, H., *J. Am. Chem. Soc.*, 1995, vol. 117, no. 41, p. 10401.
2. Yaghi, O.M., O'Keeffe, M., Ockwig, N.W., et al., *Nature*, 2003, vol. 423, no. 6941, p. 705.
3. Wilmer, C.E., Leaf, M., Lee, C.Y., et al., *Nature* Chem, 2012, vol. 4, no. 2, p. 83.
4. Herm, Z.R., Wiers, B.M., Mason, J.A., et al., *Science*, 2013, vol. 340, no. 6135, p. 960.
5. Yoon, M., Suh, K., Natarajan, S., and Kim, K., *Angew. Chem., Int. Ed. Engl.*, 2013, vol. 52, no. 10, p. 2688.
6. Lee, J., Farha, O.K., Roberts, J., et al., *Chem. Soc. Rev.*, 2009, vol. 38, no. 5, p. 1450.
7. Inokuma, Y., Yoshioka, S., Ariyoshi, J., et al., *Nature*, 2013, vol. 495, no. 7442, p. 461.
8. Giménez-Marqués, M., Hidalgo, T., Serre, C., and Horcajada, P., *Coord. Chem. Rev.*, 2016, vol. 307, p. 342.
9. Miller, S.R., Heurtaux, D., Baati, T., et al., *Chem. Commun.*, 2010, vol. 46, no. 25, p. 4526.
10. Imaz, I. and Rubio-Martinez, M., An, J., et al., *Chem. Commun.*, 2011, vol. 47, no. 26, p. 7287.
11. Zhao, J., Wei, F., Xu, W., and Han, X., *Appl. Surface Sci.*, 2020, vol. 510, p. 145418.
12. Chopra, S., Dhumal, S., Abeli, P., et al., *Postharv. Biol. Technol.*, 2017, vol. 130, p. 48.
13. Stock, N. and Biswas, S., *Chem. Rev.*, 2011, vol. 112, no. 2, p. 933.
14. Zhao, Y., Li, K., and Li, J., *Z. Natur. B*, 2010, vol. 65, no. 8, p. 976.
15. Clausen, H.F., Overgaard, J., Chen, Y.S., and Iversen, B.B., *J. Am. Chem. Soc.*, 2008, vol. 130, no. 25, p. 7988.
16. Poulsen, R.D., Jørgensen, M.R.V., Overgaard, J., et al., *Chem.-Eur. J.*, 2007, vol. 13, no. 35, p. 9775.
17. Novaković, S.B., Bogdanović, G.A., Heering, C., et al., *Inorg. Chem.*, 2015, vol. 54, no. 6, p. 2660.
18. Poulsen, R.D., Bentien, A., Graber, T., and Iversen, B.B., *Acta Crystallogr., Sect. A: Found. Crystallogr.*, 2004, vol. 60, no. 5, p. 382.
19. Li, X.H., Chen, W.L., and Wang, E.B., *Acta Crystallogr., Sect. E: Struct. Rep. Online*, 2009, vol. 65, p. m183.
20. Che, P., Fang, D., Zhang, D., et al., *J. Coord. Chem.*, 2005, vol. 58, no. 17, p. 1581.
21. Wu, J., *Acta Crystallogr., Sect. E: Struct. Rep. Online*, 2008, vol. 64, p. 583.
22. Zhang, G., Yang, G., and Ma, J.S., *Cryst. Growth & Des.*, 2006, vol. 6, no. 2, p. 375.
23. Kloubert, V. and Rink, L., *Food Funct.*, 2015, vol. 6, no. 10, p. 3195.
24. Kimura, T. and Kambe, T., *Int. J. Mol. Sci.*, 2016, no. 3, p. 336.
25. Gurtler, J.B. and Mai, T.L., in *Encyclopedia of Food Microbiology*, Batt, C.A. and Tortorello, M.L., Eds., Oxford: Academic, 2014, p. 119.
26. Tolborg, K. and Iversen, B.B., *Chem.-Eur. J.*, 2019, no. 66, p. 15010.
27. Krawczuk, A. and Macchi, P., *Chem. Centr. J.*, 2014, vol. 8, no. 1, p. 68.

28. Macchi, P., *CHIMIA Int. J. Chem.*, 2009, vol. 63, nos. 1–2, p. 29.
29. Jørgensen, M.R.V., Clausen, H.F., Christensen, M., et al., *Eur. J. Inorg. Chem.*, 2011, vol. 2011, no. 4, p. 549.
30. Jørgensen, M.R.V., Cenedese, S., Clausen, H.F., et al., *Inorg. Chem.*, 2013, vol. 52, no. 1, p. 297.
31. Dos Santos, L.H.R., Lanza, A., Barton, A.M., et al., *J. Am. Chem. Soc.*, 2016, vol. 138, no. 7, p. 2280.
32. Kubus, M., Lanza, A., Scatena, R., et al., *Inorg. Chem.*, 2018, vol. 57, no. 9, p. 4934.
33. Poulsen, R.D., Bentien, A., Chevalier, M., and Iversen, B.B., *J. Am. Chem. Soc.*, 2005, no. 25, p. 9156.
34. Jørgensen, M.R., Hathwar, V.R., Bindzus, N., et al., *IUCrJ*, 2014, vol. 1, p. 267.
35. Garino, C., Borfecchia, E., Gobetto, R., et al., *Coord. Chem. Rev.*, 2014, vols. 277–278, p. 130.
36. Pietzke, M., Meiser, J., and Vazquez, A., *Mol. Metabol.*, 2020, vol. 33, p. 23.
37. Momb, J., Lewandowski, J.P., Bryant, J.D., et al., PNAS, 2012, p. 201211199.
38. Hansen, N.K. and Coppens, P., *Acta Crystallogr., Sect. A: Cryst. Phys., Diffr., Theor. Gen. Crystallogr.*, 1978, vol. 34, p. 909.
39. Volkov, A., Macchi, P., Farrugia, L.J., et al., *XD2016, A Computer Program Package for Multipole Refinement, Topological Analysis of Charge Densities and Evaluation of Intermolecular Energies from Experimental and Theoretical Structure Factors*, 2016.
40. Allen, F.H. and Bruno, I.J., *Acta Crystallogr., Sect. B: Struct. Sci.*, 2010, vol. 66, p. 380.
41. Chandler, G.S., Wajrak, M., and Khan, R.N., *Acta Crystallogr., Sect. B: Struct. Sci., Cryst. Eng. Mater.*, 2015, vol. 71, p. 275.
42. Madsen, A., *J. Appl. Crystallogr.*, 2006, vol. 39, p. 757.
43. Hirshfeld, F.L., *Acta Crystallogr., Sect. A: Cryst. Phys., Diffr., Theor. Gen. Crystallogr.*, 1976, vol. 32, no. 1, p. 239.
44. Meindl, K. and Henn, J., *Acta Crystallogr., Sect. A: Found. Crystallogr.*, 2008, vol. 64, p. 404.
45. Korlyukov, A.A. and Nelyubina, Yu.V., *Usp. Khim.*, 2019, vol. 88, p. 677.
46. Kirzhnits, D.A., Lozovik, Yu.E., and Shpatakovskaya, G.V., *Usp. Fiz. Nauk.*, 1975, vol. 711, p. 3.
47. Bader, R.F.W., in *Atoms in Molecules. A Quantum Theory*, Bader, R.F.W, Ed., Oxford: Clarendron, 1990.
48. Stash, A. and Tsirelson, V., *J. Appl. Crystallogr.*, 2002, vol. 35, p. 371.
49. Alvarez, S., *Chem. Rev.*, 2015, vol. 115, p. 13447.
50. Dolomanov, O.V., Bourhis, L.J., Gildea, R.J., et al., *J. Appl. Crystallogr.*, 2009, vol. 42, p. 339.
51. Lee, C.-R., Wang, C.-C., Chen, K.-C., et al., *J. Phys. Chem. A*, 1999, vol. 103, no. 1, p. 156.
52. Wang, R., Lehmann, C.W., and Englert, U., *Acta Crystallogr., Sect. B: Struct. Sci.*, 2009, vol. 65, no. 5, p. 600.
53. Kotova, O., Lyssenko, K., Rogachev, A., et al., *J. Photochem. Photobiol., A*, 2011, vol. 218, no. 1, p. 117.
54. Holladay, A., Leung, P., and Coppens, P., *Acta Crystallogr., Sect. A: Found. Crystallogr.*, 1983, vol. 39, no. 3, p. 377.
55. Bader, R.F.W., *J. Phys. Chem. A*, 1998, vol. 102, p. 7314.
56. Bader, R.F.W., *Chem.-Eur. J.*, 2006, vol. 12, p. 2896.
57. Lyssenko, K.A., *Mendeleev Commun.*, 2012, vol. 22, no. 1, p. 1.
58. Espinosa, E., Molins, E., and Lecomte, C., *Chem. Phys. Lett.*, 1998, vol. 285, nos. 3–4, p. 170.
59. Espinosa, E., Alkorta, I., Rozas, I., et al., *Chem. Phys. Lett.*, 2001, vol. 336, p. 457.
60. Lysenko, K.A., Barzilovich, P.Yu., Nelyubina, Yu.V., et al., *Izv. Akad. Nauk, Ser. Khim.*, 2009, no. 1, p. 31.
61. Stock, N. and Bein, T., *Angew. Chem., Int. Ed. Engl.*, 2004, vol. 43, no. 6, p. 749.
62. Chimpri, A.S. and Macchi, P., *Phys. Scrip.*, 2013, vol. 87, no. 4, p. 048105.
63. Allendorf, M.D. and Stavila, V., *CrystEngComm*, 2015, vol. 17, no. 2, p. 229.
64. Moulton, B. and Zaworotko, M.J., *Chem. Rev.*, 2001, vol. 101, no. 6, p. 1629.

Translated by E. Yablonskaya